#1

SACLANTCEN MEMORANDUM
serial no.: SM-276

SACLANT UNDERSEA
RESEARCH CENTRE

MEMORANDUM

Inversion of seismo-acoustic real data using genetic algorithms

M. Lambert

March 1994

Page count for SM-276 (excluding Covers and Data Sheet)

Pages	Total
i–vi	6
1–40	40
	46

SACLANT Undersea Research Centre
Viale San Bartolomeo 400
19138 San Bartolomeo (SP), Italy

tel: 0187 540 111
fax: 0187 524 600
telex: 271148 SACENT I

NORTH ATLANTIC TREATY ORGANIZATION

SACLANTCEN SM-276

Inversion of seismo-acoustic real data using genetic algorithms

M. Lambert

The content of this document pertains to work performed under Project 19 of the SACLANTCEN Programme of Work. The document has been approved for release by The Director, SACLANTCEN.

Issued by:
Underwater Research Division

W.I. Roderick
Division Chief

intentionally blank page

SACLANTCEN SM-276

Inversion of seismo-acoustic real data using genetic algorithms

M. Lambert

Executive Summary: Numerical models for sound propagation are required for sonar range assessment and system performance prediction. These models are very advanced and practical applications are limited by the available knowledge of the environmental parameters. They can also be used as means of predicting ocean and geo-acoustic parameters from acoustic measurements of the sound field. Traditionally this inversion has been carried out manually through iterative forward modeling, where unknown environmental parameters are varied in a systematic fashion until a good fit is obtained between measured and modeled data. Helped by the surge in computer power it is now feasible to do such an inversion automatically. The inversion is done by minimizing an object function, a measure of the misfit between the observed and calculated sound fields based on the estimated environmental parameters. This optimization is here carried out by using a Monte Carlo method called genetic algorithms.

The aim of this memorandum is to automatically invert real transmission loss data obtained at the Tellaro site in the Bay of La Spezia, in order to determine the bottom parameters. This is the first successful attempt to do an automatic inversion on real data. Even though the inversion procedure is very efficient, we are required to assess whether the solution is physically realistic and, in the input phase, to decide how the environment should be parameterized. Thus several issues have to be addressed before an automatic inversion is available.

For the Tellaro test site it was found that at a frequency of 330 Hz only the first few meters of the sediment were important for wave propagation, and therefore information about the deeper layers can only be retrieved with high uncertainty. The standard SACLANTCEN propagation models SAFARI and SNAP have been used as forward models for the inversion. While SAFARI is more general, SNAP was found to be faster and sufficiently accurate for this inversion.

intentionally blank page

Inversion of seismo-acoustic real data using genetic algorithms

M. Lambert

Abstract: An inversion scheme for the estimation of the physical parameters of marine sediments from the pressure field measured in the water column, is presented. It is based on a global optimization technique called Genetic Algorithms. This report presents results obtained on synthetic and real data. An analysis of the uncertainties of the results is carried out to assess the reliability of the inversion.

Keywords: *a posteriori* probability distribution ∘ global optimization ∘ genetic algorithm ∘ inverse problems ∘ marine sediment

Contents

Acknowledgements: I would like to thank Peter Gerstoft, my supervisor, for his patience and for his availability at all times. It is thanks to him that my stay in Italy was so fulfilling. My thanks go also to Andrea Caiti and Rolf Inge Ambjørnsen for having processed the experimental data.

This stay would not have been possible without SACLANTCEN Summer Research Assistant Programme. I should therefore like to thank Professeur Arques, responsible for this programme in France, together with Dominique Lesselier, my supervisor. I am most grateful also for the care with which Lesselier followed my work and corrected this manuscript.

1 Introduction

At the present time, inversion problems in general are being considered not only in the field of seismo-acoustics but also in medical imaging and civil engineering. The mode of operation is the following: a known signal (which can be a CW source or a time source) interrogates an unknown environment (human body, earth, structure, ocean floor) whose response is measured on receivers (with known positions). Physical characteristics are then extracted from this response. Here, our work aims to retrieve the physical characteristics of the ocean floor from its response to an acoustic source placed above it, which involves solving a non-linear problem. The inversion is posed as an optimization problem. The different techniques developed during the last few years to solve similar problems can be grouped in two families:

Local search Like a gradient method or a Gauss-Newton method, which may fail when the starting model is far from the true model (for example, we can get stuck in a local minimum).

Global optimization Like simulated annealing or genetic algorithms, which is based on a random walk in model space and the use of a transition probability which – at least theoretically – allows us to jump out of a local minimum and go to a lower one. A good description of the state-of-the-art can be found in Scales et al. (1992).

In this report the inversion code using genetic algorithms (GA) described by Gerstoft (1993; 1994), is used to solve the above problem, i.e. the ocean floor identification, in different domains (wave number and range domains) from field data recorded either on a vertical or a horizontal array of hydrophones or on an array of geophones. The inversion is posed as an optimization problem, which is solved by a directed Monte Carlo search using genetic algorithms.

Genetic algorithms, see e.g. Davis (1991), are based on an analogy with biological evolution. these have already provided promising results in the seismic community (Stoffa and Sen, 1991; Sen and Stoffa, 1992; Sambridge and Drijkoningen, 1992; and Scales et al., 1992), a first application to ocean acoustic problems was published only recently (Gerstoft, 1993). The genetic algorithm is formulated by steady-state reproduction without duplicates. For the selection of 'parents', the object function is scaled according to a Boltzmann distribution with a 'temperature' equal to the fitness of one of the members in the population. An analysis of the uncertainties of the result is carried out by computing the response from many environmental parameter sets, hereby the *a posteriori* probabilities of the model parameters can be estimated. Thus, both uniqueness and uncertainty of the model parameters are

assessed.

Inversion methods are generally formulated independently of forward modeling routines. In this particular study, the genetic algorithm is applied to retrieve physical characteristics of the range-independent seafloor from the knowledge of the pressure field measured on receivers at fixed depth and varying range from a CW source. The forward modeling routines used are SNAP (Jensen and Ferla, 1979) (SACLANTCEN normal-mode acoustic propagation model) and OASES, which is an updated version of SAFARI (Schmidt, 1987) (Seismo–acoustic fast field algorithm for range-independent environments).

The aim of the present report is to invert the transmission loss data obtained at the Tellaro site, off La Spezia, Italy, see Sect. 5, by the use of genetic algorithms (Gerstoft, 1993) In order to do this it was necessary first to do a feasibility analysis on synthetic data generated with OASES.

2
Principles of the inversion

2.1. OPTIMIZATION

An inversion problem can be formulated as an optimization problem. The goal is to find the model vector $\mathbf{m}$ that minimizes or maximizes a function ϕ called the object function, cost function, objective function or fitness (genetic algorithm terminology). The choice of the fitness formulation depends both on the problem at hand and on the measured data available (in our case, the amplitude of the pressure field vs. range). We have chosen a quadratic deviation

$$\phi(\mathbf{m}) = \frac{\left\| \, |d_{\text{obs}}| - r|d_{\text{cal}}(\mathbf{m})| \, \right\|^2}{\left\|d_{\text{obs}}\right\|^2}, \tag{1}$$

where

$$r = \frac{\left\|d_{\text{obs}}\right\|}{\left\|d_{\text{cal}}(\mathbf{m})\right\|}. \tag{2}$$

Here $\|\cdot\|$ is the least square norm of a vector and $|\cdot|$ is the absolute value of each observation in a vector. d_{obs} and d_{cal} are vectors containing the observed and calculated data, $\mathbf{m}$ is the model vector containing the physical parameters, and r, given by Eq. (2), being a normalization coefficient which allows us to work only with the shape of the pressure field.

The function $\phi(\mathbf{m})$ could be highly oscillatory and then difficult to optimize by the classical local methods. Two solutions are available:

Re-parametrization By choosing another set of parameters a smoother object function is obtained and the number of local minima is decreased. In this case, local methods are often used to retrieve parameters because of their convergence speed (Rajan et al., 1987; Rajan, 1992a; 1992b; Caiti et al., 1993). This re-parametrization becomes very difficult with a high number of parameters.

Global optimization This allows the introduction of an object function with a highly irregular behavior. Earlier, simple Monte Carlo methods were used, with each iteration decoupled from the others; later, directional search methods such as Simulated Annealing (SA) (Mosegaard and Vestergaard, 1991; Collins et al., 1992) and Genetic Algorithms (GA) (Sen and Stoffa, 1992; Sambridge and Drijkoningen, 1992) have been applied.

2.2. GENETIC ALGORITHMS

GA and SA are based on a random walk in the search space, like a Monte Carlo method, but, unlike Monte Carlo methods, a probability rule is used to guide the search. Therefore, these two methods are termed directed Monte Carlo methods. We briefly present below the SA theory in order to explain the role of the cooling temperature used during the search. As a matter of fact, GA can be used with such a temperature to combine advantages of SA with those of GA.

SA is similar to the cooling of a liquid to obtain a crystal; the temperature must decrease slowly to allow the atoms to attain their minimum energy. In SA, at the beginning, a model vector is chosen randomly, its energy taken as a measure of the data fit being calculated at each step. When the energy is decreasing, the new model is better and is kept; when the energy is increasing, the model is accepted with a probability related to the temperature. The mathematical expression of the probability is $\exp(-\delta E/T)$ (Boltzmann formulation), where δE is the energy change and T the temperature. When T approaches infinity, all configurations are accepted, which allows moving from a local minimum. When T approaches zero, only lower energy states are accepted and the system may become trapped in a local minimum. The temperature is decreased during the execution of the algorithm in order to allow the system to proceed to the global minimum state. The main difficulty is the choice of T and its cooling schedule. Indeed, if the cooling is too fast, the system can be trapped in a relative minimum, and, if it is too slow, the calculation time becomes large.

GA is based on genetic theory. The system we work with is discretized into M parameters in a model vector $\mathbf{m}$ called a chromosome. Each parameter m_j, $j = 1, \ldots, M$, can take 2^{n_j} values (Fig. 1) between the lower bound $m_j^{\min}$ and the upper bound $m_j^{\max}$ according to an *a priori* distribution (Gaussian, rectangular — which was chosen here — or some other distribution). Each parameter is called a gene in accordance with the natural terminology of the genetic theory. We have

$$m_j = m_j^{\min} + i_j \, \Delta m_j, \quad i_j = 0, \ldots, 2^{n_j} - 1, \tag{3}$$

where

$$\Delta m_j = \frac{m_j^{\max} - m_j^{\min}}{2^{n_j} - 1} \, . \tag{4}$$

A major difference between GA and SA is that GA is using q model vectors at the same time where q is the population size while SA is using only one. GA essentially consists of three operations: selection, crossover and mutation.

Selection In order to establish a new population, also with q members, fq parents must be selected, $0 < f < 1$. The choice is made with a probability proportional to the fitness of its members. The simplest probability is given by

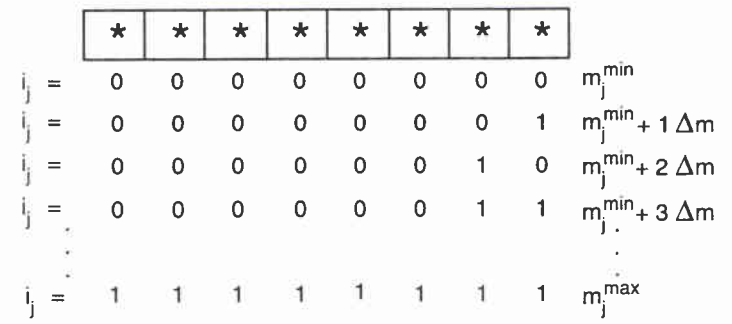

Figure 1 *Binary coding of model parameters.*

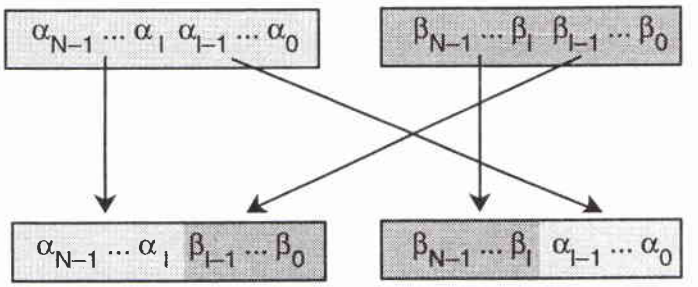

Figure 2 **Crossover** *is a binary exchange of l bits between the binary codes for two model parameters. l is chosen randomly.*

$$p_k = \frac{1 - \phi(\mathbf{m}^k)}{\sum_{l=1}^{q} \left[1 - \phi(\mathbf{m}^l)\right]}, \quad k = 1, \ldots, q. \tag{5}$$

The introduction of the temperature parameter T, as in SA, gives us the opportunity to stretch the probability and to improve the performance of the algorithms (Stoffa and Sen, 1991). Indeed, at the first stage of the procedure, by stretching the fitness we avoid selecting as parents only those members with the better fit, which would otherwise tend to dominate the population; later in the procedure, this stretching leads to a better discrimination between models with very close fitness. In order to take into account this new parameter, the probability is rewritten as

$$p_k = \frac{\exp[-\phi(\mathbf{m}^k)/T]}{\sum_{l=1}^{q} \exp\left[-\phi(\mathbf{m}^l)/T\right]}, \quad k = 1, \ldots, q. \tag{6}$$

As with SA, the choice of the temperature is difficult. It must be neither too high nor too low, and a good compromise is a temperature of the same magnitude as the object function, here $T = \min[\phi(\mathbf{m}^k)]$. During the procedure, the fitness decreases as the temperature decreases.

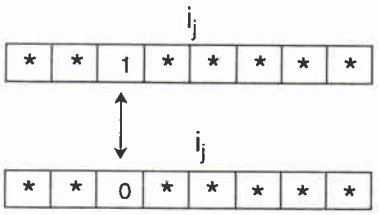

Figure 3 Mutation *is a random change of one bit.*

Crossover Once the selection is made (cf. Fig. 2), the parents are mixed together by partial exchange of genes to obtain two children with a crossover probability p_x, or the children copy from each parent with a probability of $1 - p_x$. The crossover point is chosen randomly in the interval $[1, N-1]$ where N is the number of bits used in the coding. Different techniques are available to perform this crossover of the population, e.g. the single-point crossover where the entire chromosome is used once, and the multiple-point crossover where the chromosome is divided into genes related to each parameter on which the crossover is applied.

Mutation This is a random change of bit in the model vector to better explore the whole search space (Fig. 3).

2.3. A POSTERIORI STATISTICS

During the procedure, all samples of the search space are stored and used to estimate the *a posteriori* probabilities. For a system of N parameters, the result is a N-dimensional space. Many solutions are available to display a part of this probability (see Tarantola, 1987; Frazer and Basu, 1992). We choose to use the marginal probability density function. The samples are ordered according to their energy and the probability distribution is written using the Boltzmann distribution for the optimization.

The difficulty is to choose the value of the temperature: taking it equal to the fittest sample favors the fittest part of the samples, whereas taking it equal to the least fit penalizes the best fit. A good choice, shown by experience, seems to be to use a temperature equal to the average of the best 50 examples. The probability for the kth model vector is given by

$$s(\mathbf{m}^k) = \frac{\exp\left[-\phi(\mathbf{m}^k/T)\right]}{\sum_{l=1}^{N_{\text{obs}}} \exp\left[-\phi(\mathbf{m}^l/T)\right]}. \tag{7}$$

A marginal probability distribution to obtain the value κ for each ith parameter can be calculated according to

$$s_i(m_i^k = \kappa) = \frac{\sum_{k=1}^{N_{\text{obs}}} \exp\left[-\phi(\mathbf{m}^k/T)\right] \delta(\mathbf{m}_i^k = \kappa)}{\sum_{l=1}^{N_{\text{obs}}} \exp\left[-\phi(m^l/T)\right]}, \tag{8}$$

where N_{obs} is the number of observed data and T the temperature.

The *a posteriori* mean value and covariance of the model parameters can also be estimated:

$$E(\mathbf{m}) = \sum_{k=1}^{N_{\text{obs}}} \mathbf{m}^k \sigma(\mathbf{m}^k), \tag{9}$$

$$\begin{aligned} C(\mathbf{m}) &= E\{[\mathbf{m} - E(\mathbf{m})][\mathbf{m} - E(\mathbf{m})]\}, \\ &= \sum_{k=1}^{N_{\text{obs}}} \mathbf{m}^k [\mathbf{m}^k]^T \sigma(\mathbf{m}^k) - E(\mathbf{m})[E(\mathbf{m})]^T. \end{aligned} \tag{10}$$

The diagonal of the covariance matrix is the variance of each parameter.

3
The forward modeling

Once all the physical parameters (density, P-velocity, P-attenuation, S-velocity, S-attenuation, source depth, receiver range and depth) of a horizontally stratified environment such as the ocean are known, it is possible to calculate the pressure field $P(r, z)$. In the case of a CW point source and receiver in the water, the pressure is determined by solving the Helmholtz equation in cylindrical coordinates (r, z) (completed by adequate boundary conditions at the air/water and water/bottom interfaces) which is given by

$$\frac{1}{r}\frac{\partial}{\partial r}\left(r\frac{\partial P(r,z)}{\partial r}\right) + \frac{\partial^2 P(r,z)}{\partial z^2} + \frac{\omega^2}{c^2(z)}P(r,z) = \frac{1}{2\pi r}\delta(r)\delta(z - z_s), \qquad (12)$$

where ω is the angular frequency, z_s the source depth and $c(z)$ the velocity profile in the water. In our optimization, two forward models, SNAP (Jensen and Ferla, 1979) and OASES (Schmidt, 1987), both developed at SACLANTCEN and based on Eq. (12), are used.

3.1. SNAP

The pressure field in an horizontally stratified and range-independent environment is separable in range and depth allowing the field to be expressed as

$$P(r, z_r, z_s) = I(r, z_r, z_s) + \tfrac{1}{4}i\sum_m \psi_m(z_s)\psi_m(z_r)H_0^{(1)}(k_m r), \qquad (13)$$

where i is the imaginary unit, ψ_m are orthogonal modes evaluated at source and receiver depth, z_s and z_r respectively, k_m is the horizontal wavenumber of the mth mode, $H_0^{(1)}()$ is the Hankel function of the first kind of zero order evaluated at range r, and $I(z_r, z_s, r)$ is the contribution from the branch line integral.

The summation in Eq. (13) is over the discrete modes, while the integral $I(z_r, z_s, r)$ represents the continuous modal spectrum which is important only for the near field. For the far field, the branch line contribution can be neglected as in the SNAP program. In this program, the environment is modeled as a three-layer medium (Fig. 4) as follows:

1. A water column of thickness h_0 with constant density ρ_0, constant attenuation β_0, arbitrary velocity profile $c_0(z)$ and two constants introduced to take into account the roughness of the water surface s_0 and the bottom surface s_1.

2. A sediment of thickness h_1 with constant density ρ_1, constant P-attenuation β_1 and arbitrary P-velocity profile $c_1(z)$.
3. An homogeneous subbottom with constant density ρ_2, P-velocity c_{2p}, S-velocity c_{2s}, P-attenuation β_{2p} and S-attenuation β_{2s}.

Also, by invoking adiabatic conditions SNAP may be used for so-called slow range-dependent environments. For more details on the theory and possibilities of this code, see the SNAP users' guide (Jensen and Ferla, 1979).

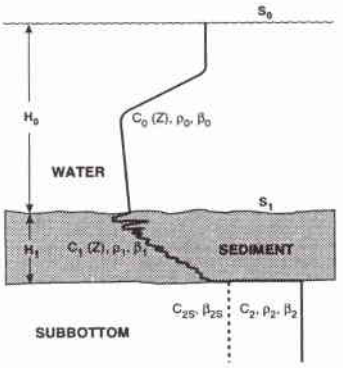

Figure 4 *Model environment for* SNAP.

3.2. OASES

This solution is based on the use of multiple integral transforms. Equation (12) is written in the wavenumber domain [see Eq. (15)] after the introduction of a zero-order Hankel transform [Eq. (14)]

$$p(k_r, z) = \int_{-\infty}^{+\infty} rP(r, z) H_0^{(1)}(k_r r) \mathrm{d}r, \tag{14}$$

$$\frac{\partial^2 p(k_r, z)}{\partial z^2} + (k^2 - k_r^2) p(k_r, z) = -\frac{1}{2\pi} \delta(z - z_s), \tag{15}$$

where k_r is the horizontal wavenumber and $p(k_r, z)$ the Green's function. Equation (15) is an ordinary differential equation, which can be easily solved once completed by the adequate boundary conditions. The inverse transform, Eq. (16), is then used to return to the range domain

$$P(r, z) = \int_{-\infty}^{+\infty} k_r p(k_r, z) H_0^{(1)}(k_r r) \mathrm{d}k_r. \tag{16}$$

At ranges greater than a few wavelengths from the source, the Hankel function in Eq. (16) is accurately approximated by its asymptotic form

$$H_0^{(1)}(k_r r) \approx \sqrt{\frac{2}{\pi k_r r}} \exp\left[i(k_r r - \tfrac{1}{4}\pi)\right], \tag{17}$$

and Eq. (16) can be rewritten as

$$P(r,z) \approx \frac{1}{\sqrt{2\pi r}} \exp\left(-i\frac{\pi}{4}\right) \int_{-\infty}^{+\infty} \sqrt{k_r}\, p(k_r, z) \exp(ik_r r) \mathrm{d}k_r. \tag{18}$$

This last expression for $P(r,z)$ has the form of a fourier transform, which can be rapidly computed by means of a fast fourier transform (FFT) algorithm provided the function $p(k_r, z)$ in the integrand is known. SAFARI is a powerful program, devoted to the calculation of the pressure field in a stratified medium. The medium is discretized into N layers (Fig. 5). In layer n the parameters to be given are: depth z_n, density ρ_n, P-velocity c_{Pn}, P-attenuation β_{Pn}, S-velocity c_{Sn}, S-attenuation β_{Sn}. A P-velocity profile where $1/c^2(z)$ is linearly varying with depth can also be assumed in the layers. To a first order approximation, this velocity variation is a linear profile with depth. This program can, in fact, tackle many different situations, see Schmidt (1987).

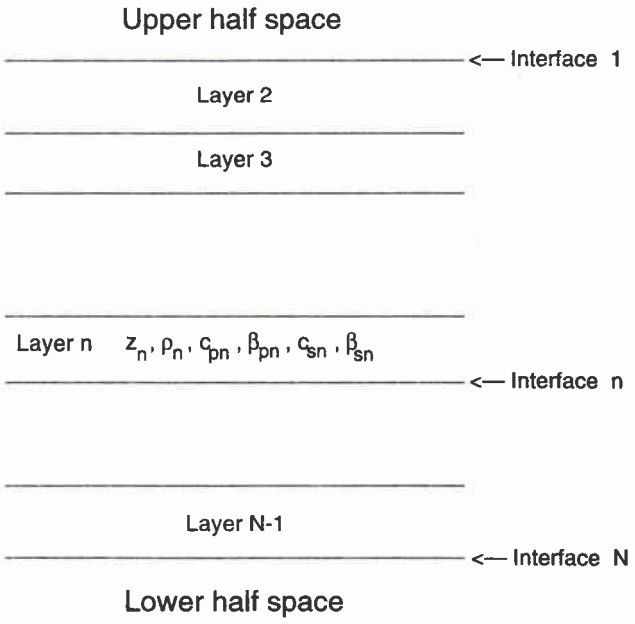

Figure 5 *Model environment for* OASES.

4

Inversion of synthetic data

In this section, the goal is to invert for the sediment parameters for a bottom, and thus a pressure field, close to the expected experimental values at the Tellaro site, see Sect. 5. The bottom at this location has a very low S-velocity, between 68 m/s and 121 m/s for the first 15 m — for details see Caiti et al. (1993). Its influence on the pressure field at the received frequency is insignificant. Thus, both the S-velocity and the S-attenuation profiles can be ignored.

Table 1 *Parameters used to obtain the synthetic dataset from* OASES. *A linearly varying P-velocity in each layer is used.*

Depth (m)	P-velocity (m/s)	P-attenuation (dB/λ)	Density (g/cm^3)
Water			
0	1523	1 E-8	1.0
15	1523	1 E-8	1.0
Sediment			
15	1490	0.40	1.5
16	1525	0.35	1.6
17	1550	0.30	1.7
20	1575	0.20	1.8
29	1700	0.15	1.9
46	1950	0.15	1.9

The synthetic pressure field vs. range used as input data was computed by OASES. The configuration consists of a water layer 15 m deep above a sediment half-space whose characteristics are given in Table 1 and Fig. 6. Source and receiver depths are 7 m and 5 m, respectively. Frequency of operation is 330 Hz. The pressure field is calculated every 2 m between 270 and 1600 m in range.

Based on our experience (Gerstoft, 1993; 1994), the genetic algorithm parameters employed in all simulations presented below are:

- Population size $q = 64$.
- Reproduction size $f = 0.5$.
- Crossover rate $p_x = 0.8$.

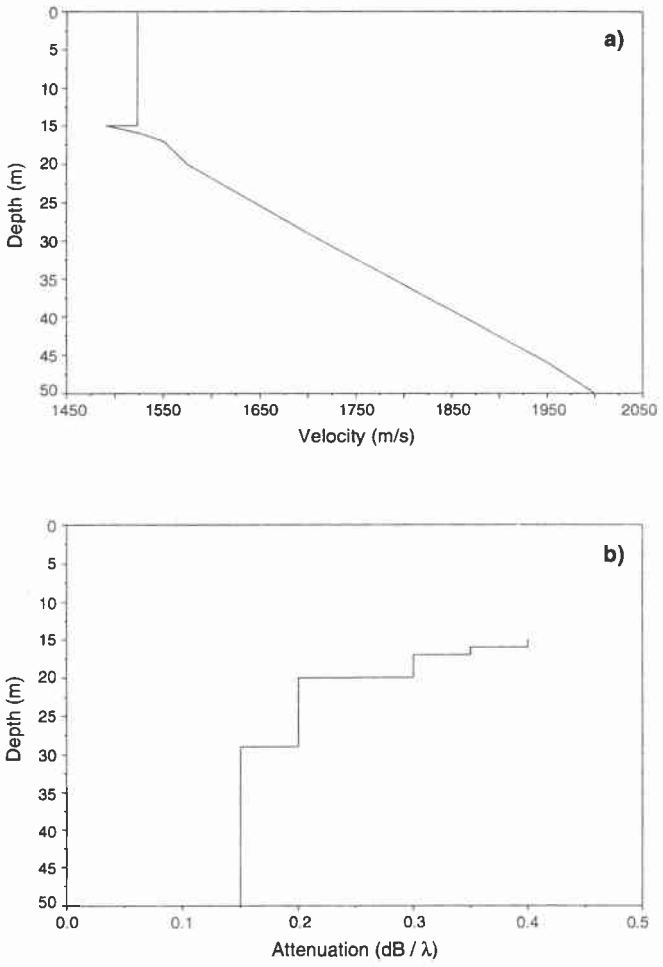

Figure 6 *P-velocity and attenuation profiles used for the synthetic case corresponding to the values of Table 1.*

- Mutation rate $p_m = 0.05$.

We did not make any studies of their influence on the covergence and results, which should be done (see Gotvald and Miya, 1993).

For each inversion 10,000 to 150,000 forward modeling runs were carried out. This corresponds to a CPU time of 1–12 hours on a DEC-3000 Alpha station. In addition to the details given below further details of each inversion is provided in the Appendix.

At the end of an inversion all the configurations computed by the genetic algorithms are kept. These configurations may be treated so as to obtain different data denoted as Best-of-All, Most Likely, Mean, which are related to the configuration which gives the lowest energy (the best fit of the data), the configuration with the most likely values of the unknowns and the configuration with the mean value of the unknowns, respectively. All the results for the pressure field, P-attenuation and P-velocity profile are computed using the Best-of-All configuration. For more details of these

different parameters see Sect. 2 and the articles by Gerstoft (1993; 1994).

4.1. METHODOLOGIES

4.1.1. Regularization

Figure 7 shows the result for the P-velocity profile without regularization (Case 1) and with regularization (Case 2).

In the first case (without regularization), the sediment is divided into 11 layers, with the value of the P-velocity in each layer being computed without enforcing any specific relation between the layers. The GA inversion with, as unknowns, the source depth and the P-velocity value in each layer provides the P-velocity profile shown in Fig. 7 (dotted line) and a source depth of 6.7 m (instead of 7 m). This profile is not realistic due to the large fluctuations in velocity, but the result for the pressure field (Fig. 8a) fits very well the synthetic data. This is probably because only the upper portion of the profile has a significant influence on the transmission loss.

Figure 9 shows the probability distribution of all parameters corresponding to the above inversion. This figure is a measure of our confidence in the result. In this case, the P-velocity in each layer is not well-determined. This confirms that the problem is ill-posed. Clearly, we need more information in order to be able to choose the most reasonable among all the possible configurations. This technique is called regularization. The choice of the regularization is connected both to the problem and to the expected solution. In our case we look for a P-velocity profile with smooth shape by the introduction of shape functions.

A shape function enables us to link some physical parameters together through a particular function. For example, it is possible to relate the source depth with the water depth in order to avoid a source depth which, for example, becomes larger than the water depth when the source must be in the water. The P-velocity profile has been modeled with only two straight lines. This can be obtained by three shape functions:

- The P-velocity at the surface of the sediment.
- The slope of the first straight line between the surface of the sediment at a depth of 15 m and the layer at a depth of 24 m, measured as the increase in velocity from 15 to 24 m.
- The slope of the straight line between 24 m and 39 m, measured as the increase in velocity from 24 to 39 m.

These 3 shape functions are used during all the simulations with SNAP and almost all with OASES.

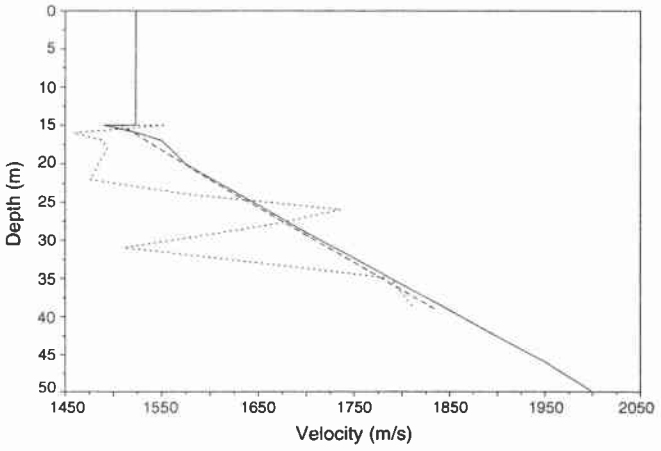

Figure 7 *P-velocity profiles (using* SNAP*) shown by the dashed line when obtained by the constrained solution (Case 2, using shape functions), and by the dotted line when obtained by the unconstrained solution (Case 1). The exact solution is the solid line.*

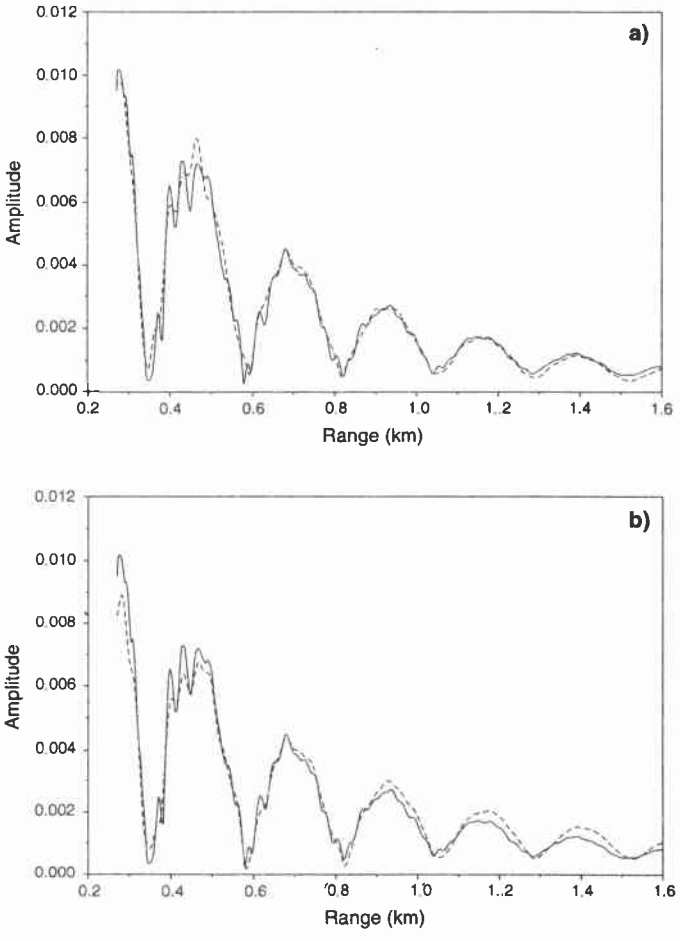

Figure 8 *Pressure field at 330 Hz. The exact solution is the solid line. a) without constraint on the P-velocity profile (Case 1, dashed line), and b) with a constrained P-velocity profile (Case 2, dashed line).* (SNAP *is used).*

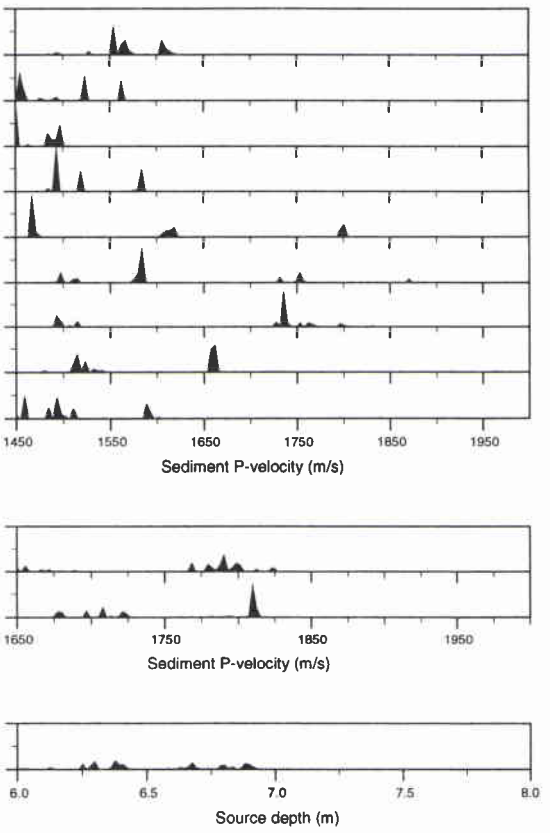

Figure 9 *Probability distribution for the eleven values of P-velocity describing the sediment and for the source depth. (Case 1,* SNAP *is used).*

It is important to note that, with these three shape functions, it is impossible to obtain the exact P-velocity and P-attenuation profiles, that is, a large model error is introduced through these shape functions, which is also a good test for the inversion program. Some other constraints could be added in the input file by reducing or increasing the interval of possible values for each parameter in each layer, to avoid, for example, the value for the last layer becoming too high or too low.

The P-velocity profile using shape functions (dashed line in Fig. 7) is well-determined. A comparison between the pressure field in the case where the P-velocity profile is constrained (Fig. 8b) and in the case where it is not (Fig. 8a) illustrates that the regularization is necessary (in fact, the energy, which measures the fit of the data to the solution, is lower for the unconstrained case than for the constrained one, see the table in the Appendix). The probability distribution (Fig. 10) shows that the regularization gives results with well-defined probabilities. The source depth found in this case is 7.02 m (instead of 7 m).

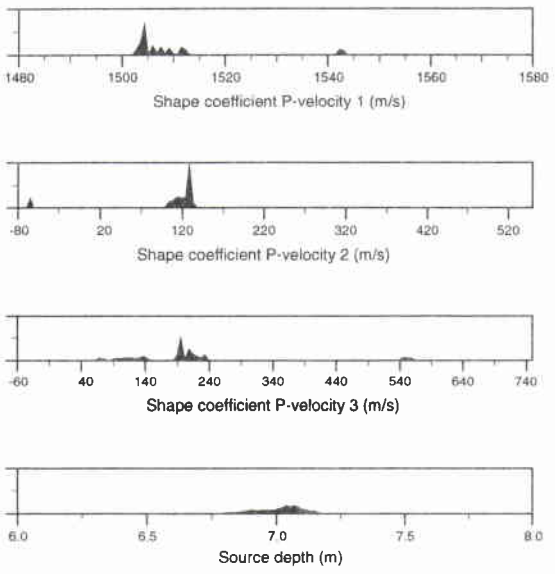

Figure 10 *Probability distributions for the three shape coefficients describing the P-velocity profile and the source depth. (Case 2,* SNAP *is used).*

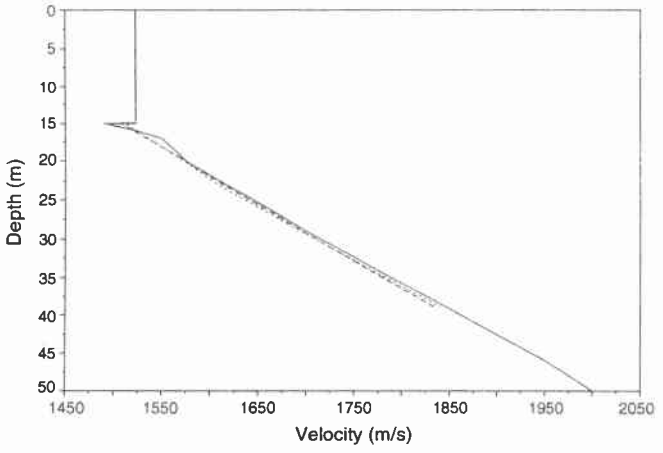

Figure 11 *P-velocity profiles obtained without weight on the field (Case 3, dashed line) and with weight by multiplying the field by* $1/\sqrt{r}$ *(Case 4, dotted line). The exact solution is the solid line. (*SNAP *is used).*

4.1.2. Weighting the response

The input data often need to be weighted in order to give special importance to certain parts of the signal. The best choice should be to multiply the amplitude of the pressure field by $\sqrt{r}$ to give the same weight to the short and long ranges since the pressure field decreases as $\sqrt{r}$ due to geometric spreading. Here, on the contrary, the data is divided by $\sqrt{r}$, which thus gives more importance to the part of the field closest to the source. This choice is imposed by the fact that the real data from the Tellaro site will be inverted (see Sect. 5). For this data set the long-range data appear to be very noisy. It is clear that, with synthetic data, this weighting reduces the information we have in the signal; we may obtain a worse solution, but it is a good test to evaluate the influence of the parameters on long-range propagation in shallow water.

Two simulations without/with weighting (Cases 3 and 4, respectively) are performed

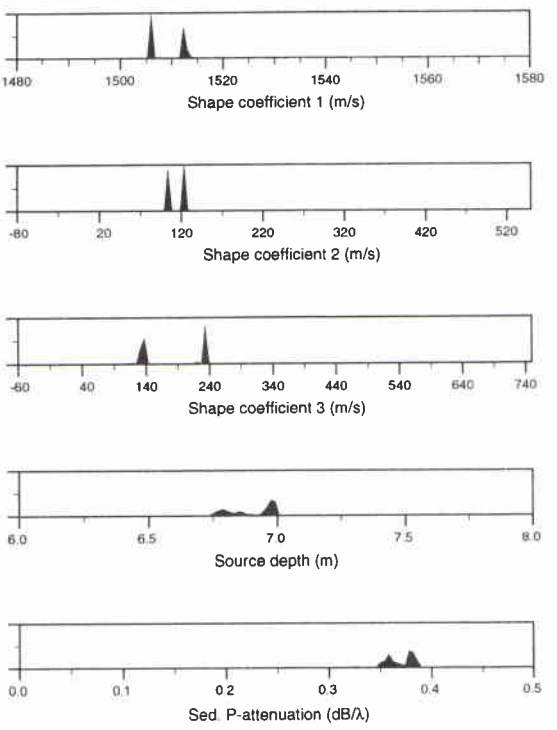

Figure 12 *Probability distribution for the three shape coefficients describing the P-velocity profile, the source depth and the P-attenuation in the sediment. The input data are not weighted. (Case 3,* SNAP *is used)*

with exactly the same unknowns, which are the P-velocity profile through the three shape coefficients, the source depth and the sediment P-attenuation. As expected, the result for the P-velocity profile is good in both cases as illustrated in Fig. 11; also the source depths are close to the exact value (see the Appendix). The results for the probability distribution are also very close to one another; only the case without weight is shown (Fig. 12). In Fig. 12 the attenuation is a free parameter, the figure will be discussed further in Sect. 4.2.1.

4.2. PARAMETERS

In this subsection, the goal is to check which parameters are important and which can be ignored, or their estimate has a low level of confidence. GA can use several different forward codes. In our case, both OASES and SNAP are being used. Each of them has its advantages and disadvantages: SNAP for example allows only a constant P-attenuation in the sediment but the code is quite fast; on the contrary, OASES allows a varying P-attenuation with depth but is rather time-consuming.

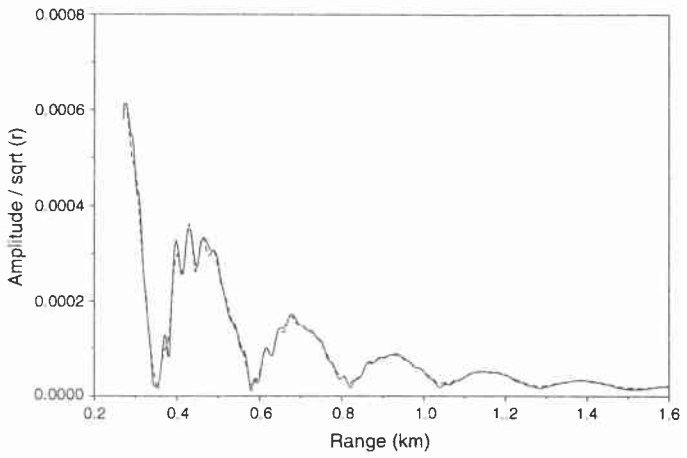

Figure 13 *Pressure field. Free parameters are the P-attenuation and P-velocity profiles and the source depth. The two profiles are introducted by four shape functions. The P-velocity in the layers is constant. The synthetic data is the solid line and the solution of the inversion is the dashed line. (Case 5,* OASES *is used).*

4.2.1. Attenuation

In this part, the goal is to verify whether:

- SNAP could be used even if it does not allow a varying P-attenuation profile and then to check its influence upon the retrieval of the other unknowns.
- OASES allows the retrieval of the P-attenuation profile.

SNAP The comparison between the pressure fields with fixed P-attenuation at 0.25 dB/λ, the average of the attenuation of the exact data (Case 2), and with free attenuation (Case 3) shows a better fit of the data when the attenuation is free (see, in the Appendix, the value of the energy). The probability distributions, given in Figs. 10 and 12, look alike in both cases except for the third shape coefficient which seems better defined when the attenuation is allowed to vary. The attenuation found by the search (0.33 dB/λ) is in between the attenuation of the upper layers, see Fig. 6b, which confirms the key role of the P-attenuation within the first few meters of the bottom ($\lambda = 5$m). When the attenuation is a free parameter it will not find the geometric average, but an average based on the importance for the wave propagation.

The P-velocity profiles given in Fig. 7 with fixed attenuation (dashed line) and in Fig. 11 with free attenuation (dashed line), look alike. Several explanations are possible. For example, the P-velocity profile is so much constrained by the shape functions that the GA has not enough freedom to find something else, or the fixed P-attenuation provides enough information to retrieve a correct P-velocity profile.

OASES Some small oscillations are observed on the synthetic data due to the P-velocity profile. As we have seen with SNAP, these oscillations cannot be fitted by the solution because of the constant P-attenuation which attenuates the signal excessively. Using OASES allows us to avoid this drawback of SNAP. Four shape coefficients are introduced to model the P-attenuation profile: the value of the P-attenuation of the first layer, the slopes of a straight line between 15 and 17 m, a second between 17 and 26 m and a third between 26 and 39 m. Note that OASES

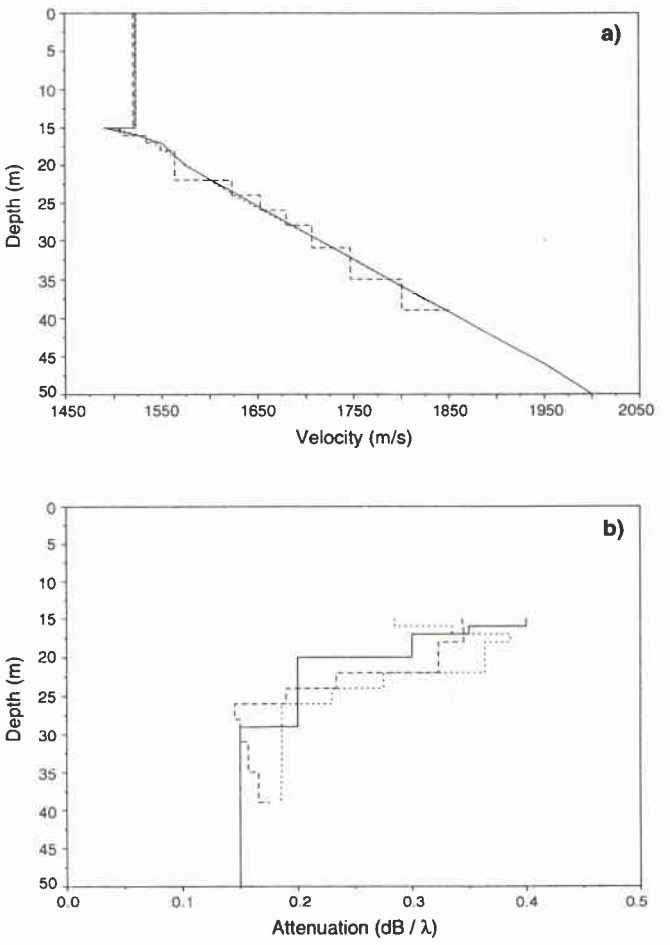

Figure 14 *P-velocity profiles (a) and P-attenuation profiles (b) in the case where the P-velocity value in each layer is constant (Case 5, dashed line) and a straight line (Case 6, dotted line). The exact solution is the solid line. (OASES is used).*

can use two different P-velocity profiles in each layer, linearly varying or stepwise, both options are tested. The linear varying, or straigth line layers, are only lineary varying to a first order approximation, see Sect. 3.2.

Constant layer (Case 5) As illustrated in Fig. 13, a varying attenuation allows a better fit of the data (results are excellent, even the small oscillations being well fitted). However, the probability distribution (Fig. 15) is not as well-determined as with SNAP. As for the P-velocity profile, it is quite good (Figs. 14a,b) but the P-attenuation profile is not very well reconstructed.

Straight line layers (Case 6) In this example linearly varying layers are hypothesized. Results are almost the same as with homogeneous layers, though to compute them takes much more time. The results are compared with the homogeneous-layer case in Figs. 14a,b.

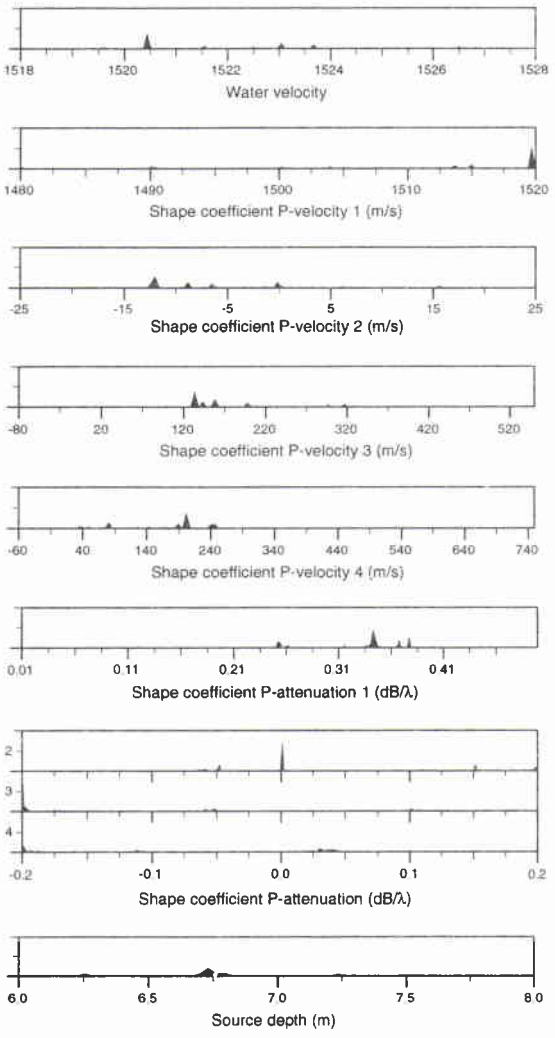

Figure 15 *Probability distributions in the case where the P-velocity is constant in the layers. (Case 5,* OASES *is used).*

4.2.2. Density

Using the same parameters as in Sect. 4.1.2 without any weighting of the data but with the density in the sediment added (Case 7), Fig. 16 (probability distribution) shows that the density is not defined as well as the other unknowns, the distribution is more flat.

The forward model used in this case is SNAP, which does not allow a varying density in the sediment. However, inversions performed with OASES, which allows varying density, provides the same result. In short, the density is not an important parameter and hence can be retrieved only with limited accuracy.

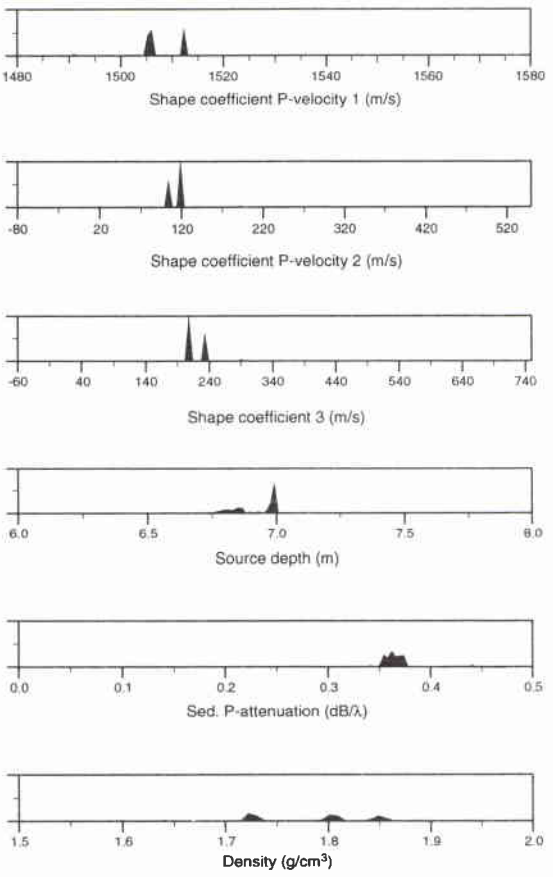

Figure 16 *Probability distributions for the three shape functions for the P-velocity profile, the source depth, the P-attenuation and the density of the sediment. (Case 7,* SNAP *is used).*

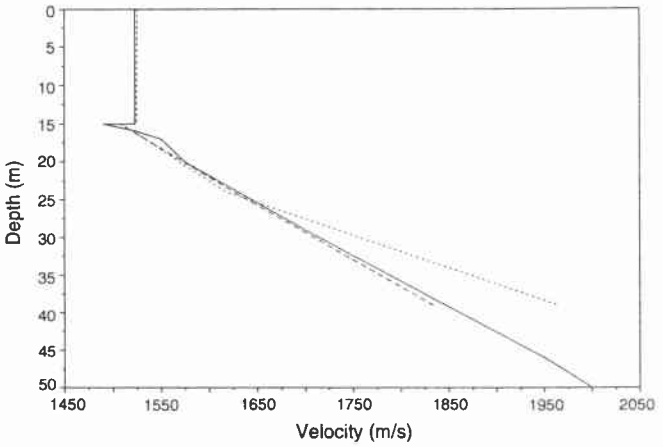

Figure 17 *P-velocity profiles. Parameters are the source depth, the P-velocity, the P-attenuation. The water velocity is constant (Case 4, dashed line) or represented by 2 parameters (Case 8, dotted line). The exact solution is the solid line. (*SNAP *is used).*

4.2.3. Water velocity

The velocity in the water column is obviously one of the most important parameters for propagation in a shallow-water environment. We use exactly the same parameters as in Sect. 4.1.2., the case without weighting of the data (Case 4), but with the velocity profile in the water added as an unknown through the velocity at the water

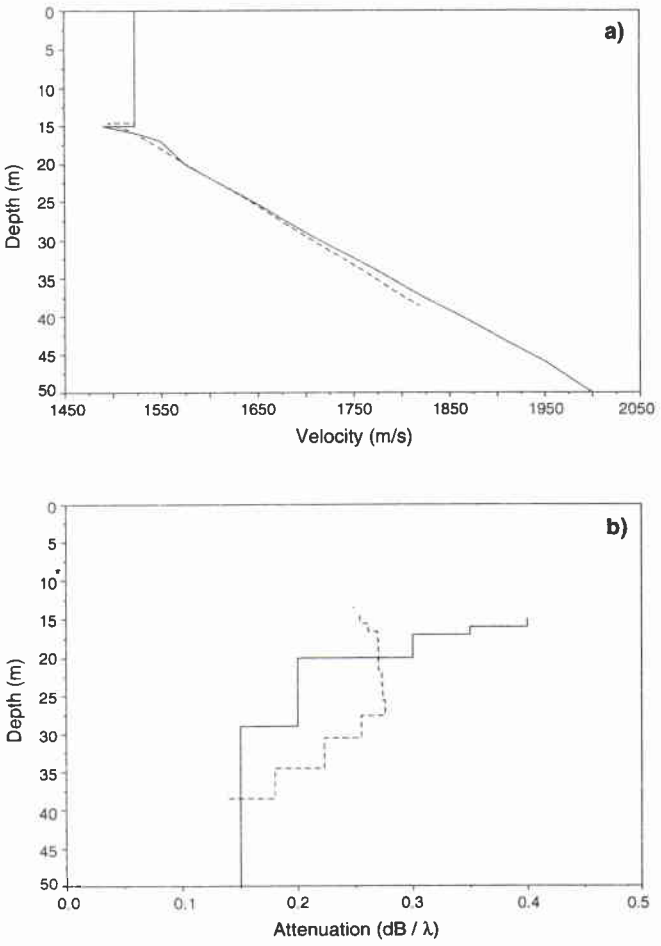

Figure 18 *The P-velocity profile (a) and the attenution profile (b) when also the water depth is a parameter (dashed line). The exact solution is the solid line. (Case 10,* OASES *is used).*

surface and at the bottom (Case 8). Both retrieved profiles are presented in Fig. 17. It may be seen that the best profiles are obtained when the water profile is not included. To include the water velocity gives 2 extra parameters which have to be determined. Further, if the slope, the difference between top and bottom, is not correct a poor fit is expected (Gerstoft, 1994). Thus it just makes the inversion more difficult, by introducing the water velocity in this case.

4.2.4. Giving more freedom to the sediment velocity

In long-range propagation, it is known that the first few meters of the sediment play a important role. To provide more freedom to the first meters, a fourth shape function is added (Case 9), which gives more freedom to the P-velocity profile at the beginning. This leads to a better fit of both the data and of the P-velocity profile. The better results are because there is now more freedom to match the profile, and also the new parameter is an important parameter.

4.2.5. Water depth

The water depth is also a very important parameter for propagation in shallow water. It should be given enough freedom so that the water depth can be retrieved from the data. OASES is used, with as parameters, the water velocity, four shape coefficients for both the P-velocity and the P-attenuation profiles, the source depth and the water depth (Case 10). The P-velocity and P-attenuation profiles are shown in Figs. 18a,b. This introduces an extra parameter in the search space, but the velocity profile is found rather well. However, the attenuation is not well retrieved.

4.3. CONCLUSIONS

Results obtained by GA using synthetic data have been discussed in this chapter. Two different forward models have been employed, SNAP and OASES. The different parameters are more or less well-determined but it is clear that shape functions are absolutely necessary to reduce the size of the search space and to regularize the problem. The P-velocity profile and the source depth are usually well-resolved but the water depth and the water-velocity profiles seem to be difficult to obtain. Also, density and P-attenuation are not well-determined. A brief comparison of the results according to the forward modeling is presented below.

- SNAP: gives good results for the P-velocity profile, the source depth and the P-attenuation (but only for the first two meters due to the fact that constant attenuation in the sediment is assumed). This is a limitation for fitting the data well. The water-velocity profile is not well-determined. The major advantage of this model is a fast computing time.
- OASES: leads to a better fit of the data due to the possibility of using a varying P-attenuation profile but the computing time increases very rapidly with the number of layers used to discretize the medium.

5

Inversion of real data

After testing the genetic algorithm on synthetic data, real data have been considered. The experiment TELLARO took place at two sites in the Gulf of La Spezia in June 1992, with the T-boat *Manning*. Data obtained at location A on the map (Fig. 19) are used.

The measurement configuration is sketched in Fig. 20: four receivers are fixed at the bottom at several depths (2, 5, 10 and 15 m) and the 330 Hz source is towed at a fixed depth of 7 m. The measurements were made both on the outgoing and on the return leg, which provides eight different sets of measurements. Among them, the recording made with the 5 m deep receiver on the return leg (Fig. 21) was chosen because of its higher signal-to-noise ratio compared to the others. As may be seen in Fig. 21, the data are very noisy and we have been obliged to smooth them. This is done by averaging the signal from six neighboring range values leading to the results of Fig. 22.

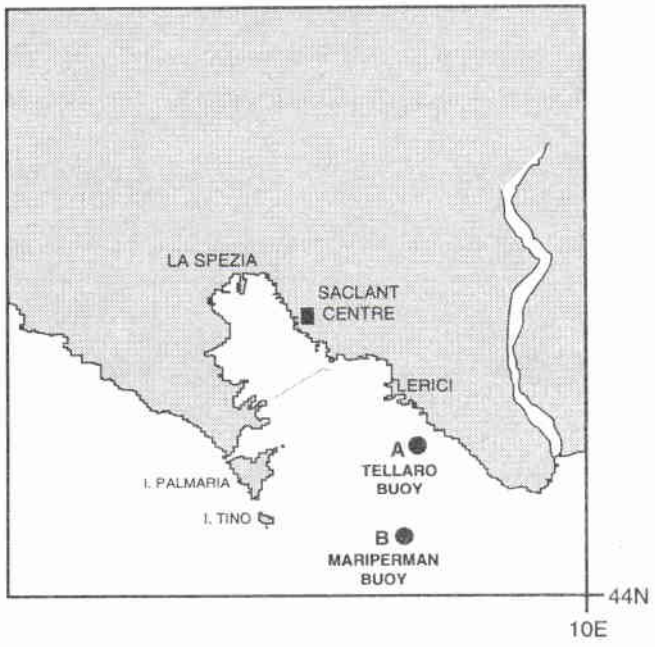

Figure 19 *TELLARO – experiment locations.*

From the XBT measurements we do have precise information on the water-velocity profile at one location (Table 2) and the water depth is 15 m. Nevertheless, in all

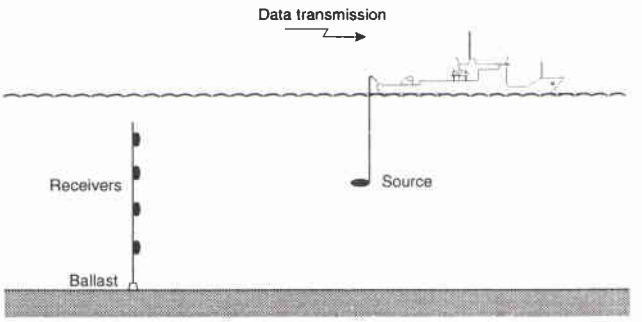

Figure 20 *Measurement configuration.*

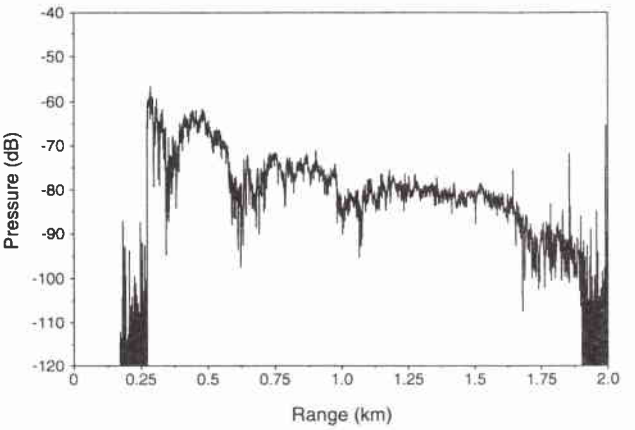

Figure 21 *Signal on the 5 m deep receiver after processing.*

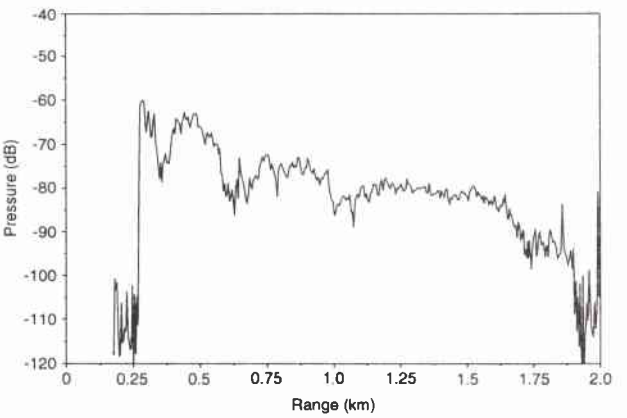

Figure 22 *Range averaged signal for a receiver at 5 m.*

our inversions we use a constant water velocity (1523 m/s); this simplification is due to the need to avoid prohibitive increase of the CPU time with the increase of the number of layers, but it obviously introduces some limitations in our reconstructions. Also, since the sea surface and the sediment surface were relatively flat, their roughness is zeroed in the initial studies. Finally, since the data are very noisy especially at long range, we only used the signal between 270 and 1600 m and weighted the data by $1/\sqrt{r}$ where r is the distance between the source and the receiver, in order to decrease the influence of the long-range data.

Table 2 *Water-velocity profile*

Depth (m)	Water velocity (m/s)
0.0	1523.0
1.1	1523.6
2.4	1523.7
3.5	1523.6
4.8	1523.8
5.9	1523.7
6.7	1524.7
8.0	1525.9
10.1	1524.3
11.2	1523.7
12.4	1523.7
13.4	1523.0
14.5	1523.0
15.0	1523.0

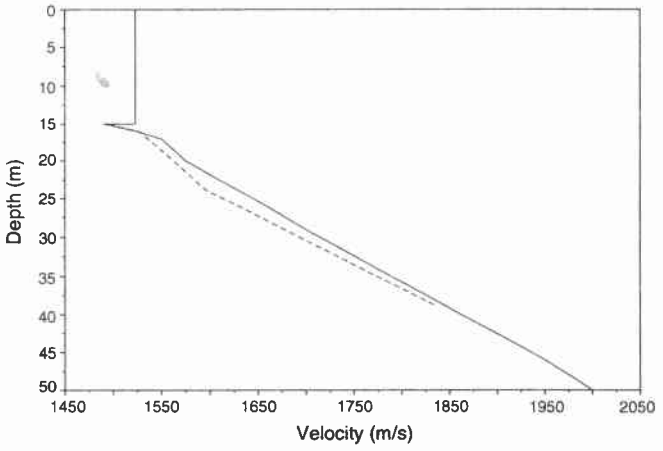

Figure 23 *P-velocity profiles. The solid line is the broadband estimated profile, the dashed line, the inverted estimate. (Case 11,* SNAP *is used).*

Some errors in the data are as follows:

- The distance is measured between the bottom ballast and the ship. This is not exactly the range but the range divided by $\cos\theta$ (with $\cos\theta \approx 1$), which introduces a small error in the range value. This error can be ignored because the range is much greater than the depth ($15/270 \ll 1$).
- The receivers are well fixed to the bottom but not at the top of the array, so they can move, which also introduces some errors in the range estimate.

Earlier a seismic broadband analysis at the Tellaro site was carried out to estimate the bottom-velocity profile. The S-wave velocity has been estimated by Caiti et al. (1993) to be about 100 m/s and therefore, its influence on the transmission loss can be ignored. The P-velocity profile has been estimated based on the Herglotz-Wiechert analysis of the reflection parabola (see e.g. Aki and Richards, 1980) and

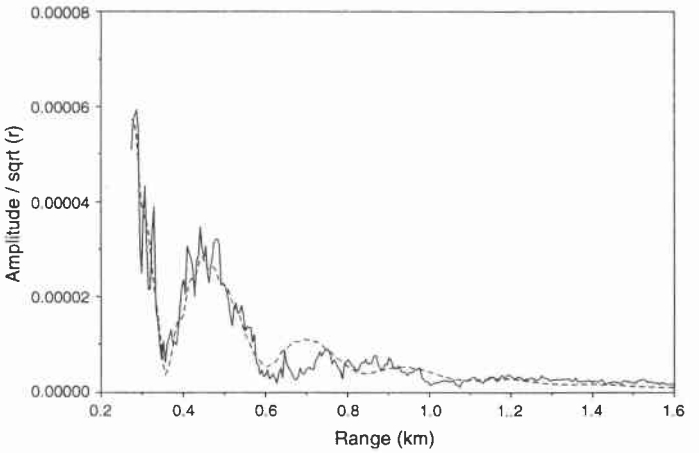

Figure 24 *Pressure field at 330 Hz obtained with the P-velocity profile and the constant P-attenuation as parameters. The dashed line is the inverted result, while the solid line is the data. (Case 11,* SNAP *is used).*

has given the broadband estimated velocity profile in Fig. 23. This profile is used for reference but it is not necessarily the correct one. As it is a broadband experiment it probably has a deeper penetration depth than the single frequency measurement.

For each inversion 10,000 to 150,000 forward modeling runs were carried out. This corresponds to a CPU time of 1–12 hours on a DEC 3000 Alpha station. In addition to the details given below further details of each inversion is provided in the Appendix.

5.1. SNAP

The SNAP input file used with GA when applied to synthetic data was modified to take into account two different P-attenuations, the first related to the sediment layer, the second to the subbottom. To start with (Case 11), we only chose as unknowns the P-velocity profile (described with four shape functions), the P-attenuation for the sediment layer and for the subbottom, all other parameters were fixed (see the table in the Appendix for input data and results). In Fig. 24 the field associated with the profiles retrieved by GA is compared with the data (Case 11). As with synthetic data, it seems to be very difficult to fit the small oscillations because of the constant P-attenuation in the sediment. Figure 23 shows the result for the P-velocity profile inversion.

As seen in Fig. 25, the probability distributions are not well-determined. If we compare this result with similar ones obtained with synthetic data (Fig. 12), we see that with real data there are no well defined peaks but many small ones. We have also some problems with the P-attenuation which is going to the maximum allowed. This indicates either that the interval of variation chosen for the parameter is underestimated or a problem in our modeling has arisen. The error in modeling could be due to hidden parameters such as a too simplistic subbottom. But, in any case, the result cannot be accepted without carrying out further investigations.

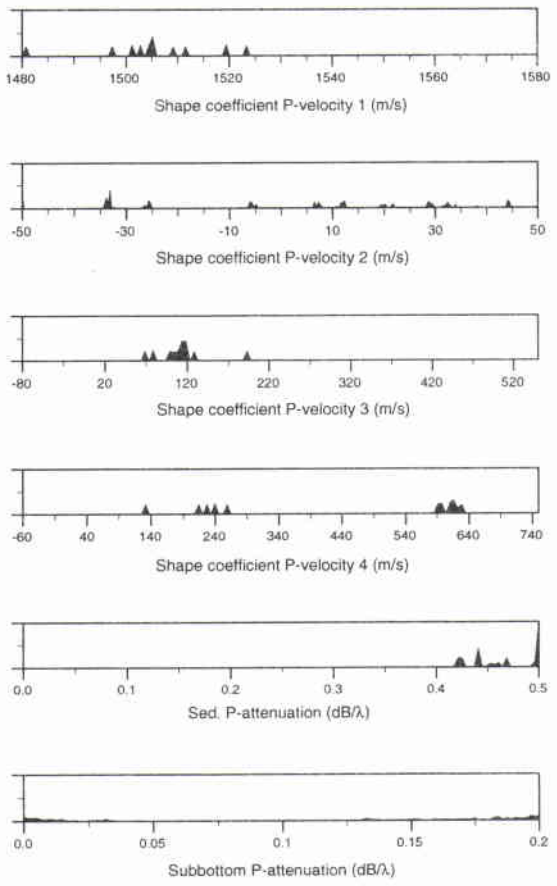

Figure 25 *Probability distributions for the four shape functions, the P-attenuations in the sediment and in the subbottom. (Case 11,* SNAP *is used).*

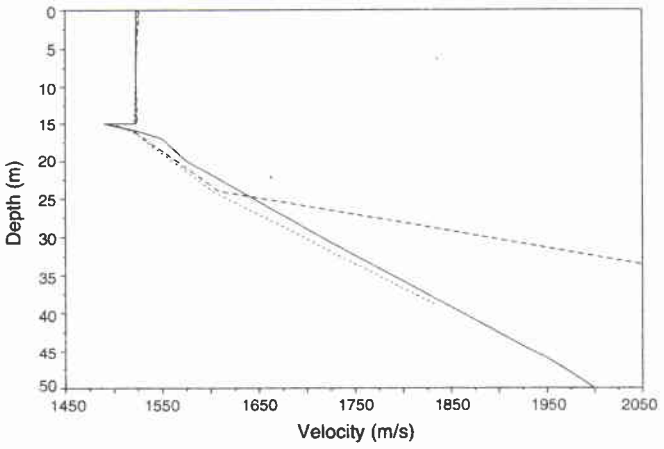

Figure 26 *P-velocity profiles for the sediment and the water. The dashed line is without constraint (Case 13), while the dotted line is with constraint on the last layer (Case 14); the solid line shows the estimated broadband solution. (*SNAP *is used).*

In this case, the attenuation is not expected to be greater than 0.5 dB/λ. So more energy loss must be introduced into the system. Adequate parameters to account for this may be the water-velocity profile (it could either increase or decrease the loss in a system), the roughness of the water surface and of the ocean bottom.

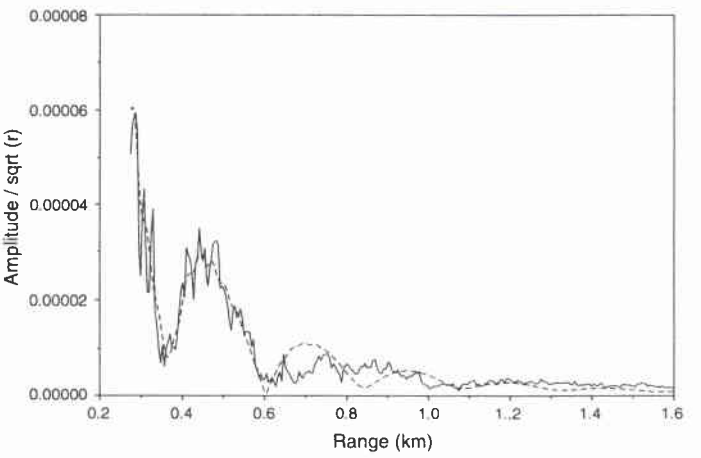

Figure 27 *Pressure field, the dashed line is obtained with constraint on the last layer, the solid line is the data. (Case 12,* SNAP *is used).*

The results for the P-velocity profile inversion, when the roughness of both the surface and the bottom, and the water-velocity profile are taken into account, are shown in Fig. 26 (Case 12 and 13). The water velocity was introduced differently from what had been done previously with the synthetic data to take into account the possibility of a varying profile. So, as parameters, we have the value of the water velocity at three points: at the surface, at 7 m (source depth) and at the bottom.

We get two different results (Fig. 26). As a matter of fact, the two runs give results very close to the broadband estimated solution for the first 5 m and diverge below. But both are made with exactly the same input file, one with more constraints on the last layer to avoid this divergence (Case 12) than the other (Case 13). These two P-velocity profiles give two pressure fields very close to one another, the differences mainly appearing at short range (between 270 and 400 m), where the subbottom is most important, and only the constrained solution is shown (Fig. 27).

In Fig. 28 the probability distribution for each parameter are shown (Case 13); the results for the case with constraints are very close and are not presented. All the values for the parameters are presented in the Appendix. Adding as unknowns the roughness and the water-velocity profile allows us to decrease the value of the P-attenuation in the sediment, even though it still seems high.

5.2. OASES

In this section the results obtained by using OASES as the forward model are presented. First, we fix all the parameters except the P-velocity and P-attenuation profiles using shape functions. The inversion is made assuming a constant (Case 14) or a straight line (Case 15) as P-velocity profile in each layer. The results are presented in Fig. 29. For the P-velocity profile, only the first 5 m are reconstructed accurately for both profiles. Beyond, there is divergence. As for the P-attenuation profile, it is not similar to the estimated broadband profile: the attenuation is approaching its maximum.

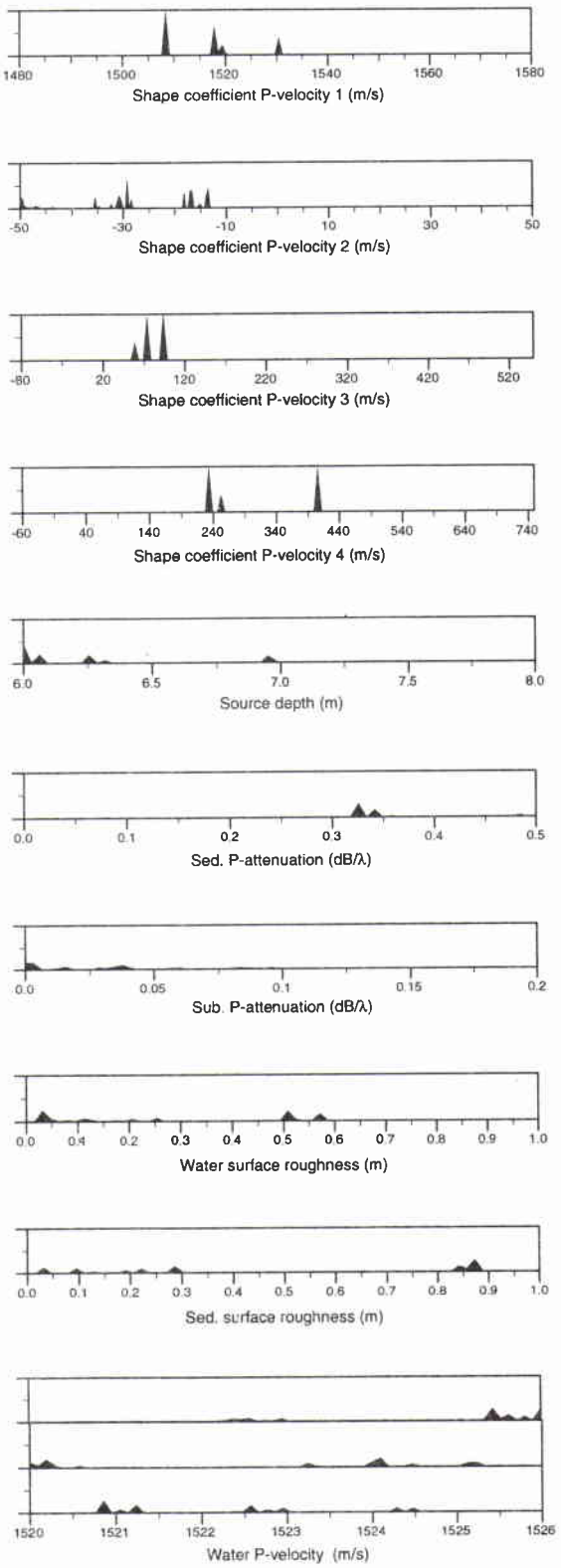

Figure 28 *Probability distribution for all parameters in the case with constraints on the last layer. (Case 12,* SNAP *is used).*

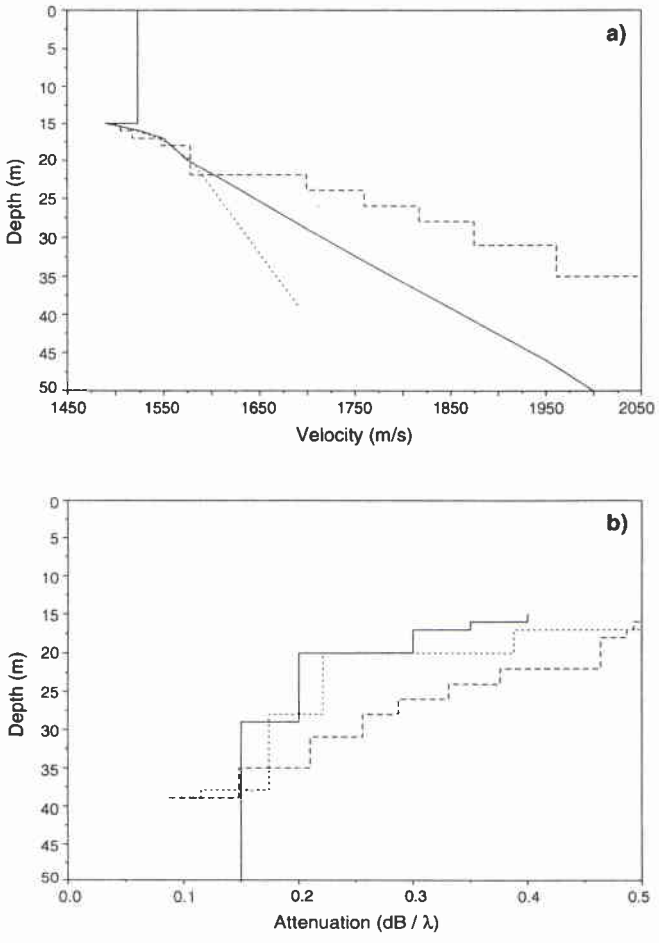

Figure 29 *P-velocity (a) and P-attenuation (b) profiles in the case where the P-velocity value in each layer is constant (Case 14, dashed line) and a straight line (Case 15 dotted line). The broadband estimate is the solid line (OASES is used).*

In the next example, we have introduced as unknowns the water velocity, the source depth, and the water depth. As with SNAP, we begin by inverting the data without constraints. The results (Case 16) are presented in Figs. 30a,b (dashed line). The P-velocity profile obtained is acceptable even though, at the end, it goes to higher values than expected. The P-attenuation is also acceptable with, at the beginning, a value of 0.3 dB/λ. The water depth (15.7 m) stays around the measured depth of 15 m.

We decided to constrain the P-velocity value of the last layer to obtain a better fit to the broadband estimated data and to observe the influence of this constraint on the other parameters (Case 17). The results, dotted line in the Figs. 30a,b, is not satisfactory because two parameters are going to their extreme values: the water depth (14 m), and the attenuation of the first layer (0.5 dB/λ). The pressure fields are very close. Only the constrained solution is shown (Fig. 31).

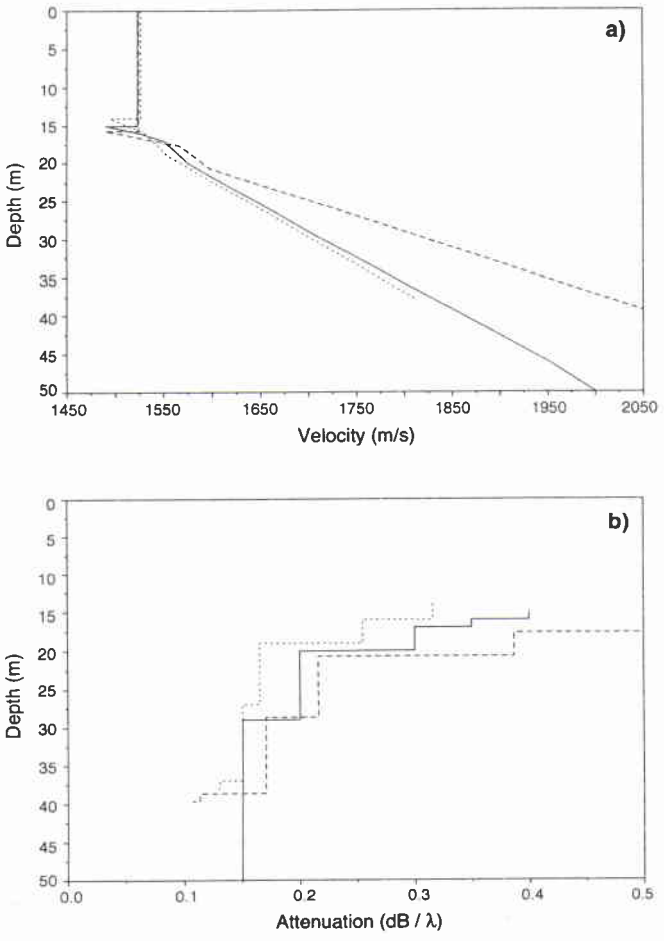

Figure 30 *P-velocity (a) and P-attenuation (b) profiles. The P-velocity value in the last layer is not constrained (Case 16, dashed line) and is constrained (Case 17, dotted line). The broadband estimated solution is the solid line (*OASES *is used).*

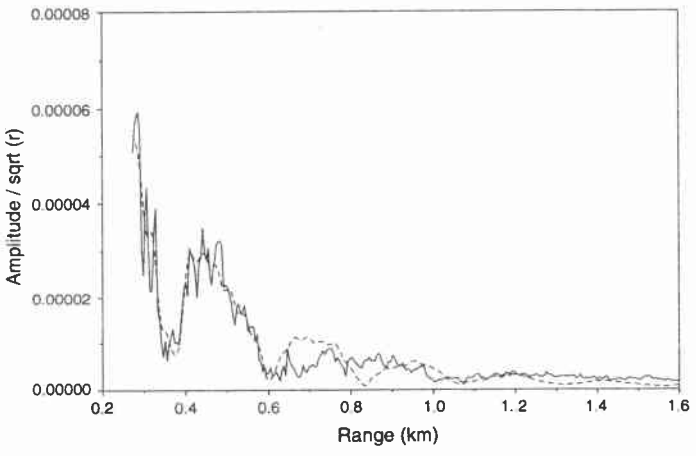

Figure 31 *Pressure field, the dashed line is obtained with constraints on the last layer, and the solid line is the data. (Case 16,* OASES *is used).*

5.3. CONCLUSIONS

The results presented in this chapter show the difficulty of inverting the pressure field without any information on the parameters and their values. If we just trust the

pressure field, all solutions presented could be good, so some extra information to select one solution over the other is needed. To do this, we worked with a probability distribution but the results with real data are not as good as expected.

The P-velocity profile can be relatively well-determined for the first few meters of the sediment. As a matter of fact, all simulations give the same behavior for the first 5 m, whereas, beyond 5 m, this profile has less influence on the field and thus this part is difficult to estimate. The deepest section of the velocity profile and the attenuation profile, is related to the small oscillations we observe on the signal, which are not very well fitted by the solution. The small oscillations are due to the heigher modes, which mainly progate in the sediment. The disagreement in the small oscillations could be due to the following reasons:

- The chosen cost function does not favor the small oscillations, but, on the contrary, it favors the large oscillations which are related to source and receiver positions and water depth.
- The retrieved P-attenuation profile, which is not well-determined, can be a bad solution. If the attenuation is high the higher modes will be damped and thus the small oscilations will not be matched.

It is possible we have been trying to fit the transmisson loss curve too closely. Maybe, we should only fit the gross features, and it is possible only to retrieve the parameters for the first few meters of the sediment.

6
Conclusions

A global inversion technique for the estimation of parameters in marine environment from the measured acoustic pressure field has been considered. Results are presented to evaluate its efficiency both on synthetic and on real data.

Some topics regarding the inversion procedure deserve more attention:

- Regularization has been introduced via the shape functions. They allow the unknown parametersto to be described and linked together using a lesser number of coefficients in order to reduce the search space. Using such shape functions has improved the reconstruction but we have only chosen straight lines as shape functions and it remains to be seen what could happen if we took some other shape functions.
- *A posteriori* distribution has been used as a measurement of how much we trust in the solution. This gives good results with synthetic data, well-determined spikes at almost the right place, but it is more difficult to obtain well-defined spikes, probably due to noise in the data and wrong discretizations.
- The population evolution depends on parameters often called auxiliary parameters (population size q, reproduction size f, crossover rate p_x and mutation rate p_m. As is well-known, the convergence speed and perhaps the estimated solution depend on the values of the auxiliary parameters. A study of their influence should in principle be done for each inversion case.

The results obtained with the application of the inversion technique upon synthetic data have shown the difficulty of finding a good agreement for all the parameters but they do allow us to evaluate the importance of these parameters on the pressure field. The work on real data has confirmed the importance of measurement quality and the difficulty of finding the correct solution among all admissible results. In both cases, the P-attenuation profile seems to be difficult to retrieve and it seems that the P-velocity profile plays only an important role for the first few meters.

Resolution of the first few meters of the bottom are probably sufficient for most underwater acoustic applications, but to resolve the parameters at greater depths the pressure field measured near the source should be used (in our case we were at 44 wavelengths from the source). This allows more signal coming from the deepest part of the sediment.

In order to speed up the forward computations, the Green's function in the spectral wave number domain should be used as data. This is possible with the OASES model. The advantage of using this domain is that we can limit the forward

modeling to, say, 100 wave numbers as opposed to about 1000 wave numbers for modeling of pressure in the range depth domain. It gives a speed-up of factor 10.

Finally, it is important to note that the automatic inversion presented here is the last in a long chain of events. If there are errors in one of the other chains this inversion will fail. The experiment should be performed correctly and the transformation of the data from the observed domain to the frequency-range domain should also be done correctly.

References

Aki, K. and Richards, P.G., 1980. Quantitative Seismology: Theory and Methods. San Francisco, CA, W.H. Freeman. [ISBN 0-7167-1059-5]

Caiti, A., Akal, T. and Stoll, R.D., 1993. Shear wave velocity in seafloor sediments by inversion of interface wave dispersion data, SACLANTCEN SR-205. La Spezia, Italy, SACLANT Undersea Research Centre. [AD B 174 744]

Collins, M.D., Kuperman, W.A. and Schmidt, H., 1992. Non linear inversion for ocean-bottom properties. *Journal of the Acoustical Society of America*, **92**, 2770–2783.

Davis, L., 1991. Handbook of Genetic Algorithms. New York, NY, Van Nostrand Reinhold. [ISBN 0-442-00173-8]

Frazer, L.N. and Basu, A., 1992. Inversion by statistical physics with an application to offset VSP. Submitted to *Geophysical Journal International.*

Gerstoft, P., 1993. Inversion of seismo-acoustic data using genetic algorithms and *a posteriori* probability distributions, SACLANTCEN SM-272. La Spezia, Italy, SACLANT Undersea Research Centre. and *Journal of the Acoustical Society of America*, **95**, 1994: 770–782.

Gerstoft, P., 1994. Global inversion by genetic algorithms for both source position and environmental parameters. To appear in *Journal of Computational Acoustics.*

Gotvald A. and Miya K., 1993. Meta-optimization and inverse problems of eddy current testing. 9th Compumag, Miami, 538–539.

Jensen, F.B. and Ferla, M.C., 1979. SNAP: the SACLANTCEN normal-mode acoustic propagation model, SACLANTCEN SM-121. La Spezia, Italy, SACLANT Undersea Research Centre. [AD A 067 256]

Mosegaard, K. and Verstergaard, P.D., 1991. A simulated annealing approach to seismic model optimization with sparse prior information. *Geophysical Prospecting*, **39**, 599–611.

Rajan, S.D., Lynch, J.F. and Frisk, G.V., 1987. Perturbative inversion methods for obtaining bottom geoacoustic parameters in shallow water. *Journal of the Acoustical Society of America*, **82**, 998–1017.

Rajan, S.D., 1992a. Determination of geoacoustic parameters of the ocean bottom — data requirements. *Journal of the Acoustical Society of America*, **92**, 2126–2140.

Rajan, S.D., 1992b. Waveform inversion for the geoacoustic parameters of the ocean bottom. *Journal of the Acoustical Society of America*, **91**, 3228–3241.

Sambridge, M. and Drijkoningen, G., 1992. Genetic algorithms in seismic waveform inversion. *Geophysical Journal International*, **109**, 323–343.

Scales, J.A., Smith, M.L. and Fischer, T.L., 1992. Global optimization methods for multimodal inverse problems. *Journal of Computational Physics*, **103**, 258–268.

Schmidt, H., 1987. SAFARI: Seismo-acoustic fast field algorithm for range-independent environments: User's guide, SACLANTCEN SR-113. La Spezia, Italy, SACLANT Undersea Research Centre. [AD A 200 581]

Sen, M.K. and Stoffa, P.L., 1992. Rapid sampling of model space using genetic algorithms: examples from seismic waveform inversion. *Geophysical Journal International*, **108**, 281–292.

Stoffa, P.L. and Sen M.K., 1991. Nonlinear multiparameter optimization using genetic algorithms: inversion of plane-wave seismograms. *Geophysics*, **56**, 1794–1810.

Tarantola A., 1987. Inverse Problem Theory: Methods for Data Fitting and Model Parameter Estimation. Amsterdam, Elsevier. [ISBN 0-444-42765-1]

Appendix A

Table of results

This appendix provide details of the inversion used in this report. For each result we have six columns which are:

- The case number, the forward model used and for OASES the P-velocity profile in a layer.
- Y(es) or N(o) to show if the data are weighted or not.
- The energy calculated with the expression (Eq.1) for the Best-of-All configuration.
- The iteration number and the population number. The total number of forward modeling runs is the product of these two numbers.
- The list of the unknown parameters with their results for the Best-of-All configuration.
- The list of the known parameters with their given values.

Table A1 *Parameters*

Case	Weighting	Energy	Iter. Pop.	Variable parameters	Constant parameters
1 SNAP	N	8.95e-3	5000 3	P-vel (12 values) source depth 6.66 m	water depth 15 m water vel 1523 m/s density 1.7 g/cm^3 P-att 0.25 dB/λ
2 SNAP	N	1.21e-2	5000 16	P-vel (3 shape funcs.) source depth 7.02 m	water depth 15 m water vel 1523 m/s density 1.7 g/cm^3 P-att 0.25 dB/λ
3 SNAP	N	6.83e-3	5000 3	P-vel (3 shape funcs.) source depth 6.99 m P-att 0.33 dB/λ	water depth 15 m water vel 1523 m/s density 1.7 g/cm^3
4 SNAP	Y	6.29e-3	5000 3	P-vel (3 shape funcs.) source depth 6.70 m P-att 0.37 dB/λ	water depth 15 m water vel 1523 m/s density 1.7 g/cm^3
5 OASES[1]	Y	2.63e-3	10000 15	P-vel (4 shape funcs.) source depth 6.73 m P-att (4 shape funcs.) water vel 1520.4 m/s	water depth 15 m density 1.7 g/cm^3
6 OASES[2]	Y	4.32e-3	5000 10	P-vel (4 shape funcs.) source depth 6.92 m P-att (4 shape funcs.) water vel 1523.7 m/s	water depth 15 m density 1.6 g/cm^3
7 SNAP	N	4.61e-3	5000 3	P-vel (3 shape funcs.) source depth 6.99 m P-att 0.36 dB/λ density 1.80 g/cm^3	water depth 15 m water vel 1523 m/s
8 SNAP	N	6.93e-3	5000 3	P-vel (3 shape funcs.) source depth 7.16 m P-att 0.38 dB/λ density 1.87 g/cm^3 water vel (top) 1525.3 m/s water vel (bot)1524.4 m/s	water depth 15 m
9 SNAP	Y	5.26e-3	5000 3	P-vel (4 shape funcs.) source depth 6.98 m P-att 0.38 dB/λ	water depth 15 m water vel 1523 m/s density 1.7 g/cm^3
10 OASES[1]	Y	5.98e-3	3000 6	P-vel (4 shape funcs.) source depth 7.02 m P-att (4 shape funcs.) water depth 14.6 m water vel 1523 m/s	density 1.7 g/cm^3

[1] Constant layer. [2] Straightline layer.

Table A1 *(Continued) Parameters*

Case	Weighting	Energy	Iter. Pop.	Variable parameters	Constant parameters
11 SNAP	Y	5.64e-2	3000 15	P-vel (4 shape funcs.) P-att sed. 0.5 dB/λ P-att bot. 0.01 dB/λ	water depth 15 m water vel 1523 m/s density 1.7 g/cm^3 source depth 7.00 m
12 SNAP	Y	5.39e-2	3000 3	P-vel (4 shape funcs.) P-att sed. 0.39 dB/λ P-att bot. 0.12 dB/λ source depth 6.13 m roughness (top) 0.03 m roughness (bot) 0.35 m water vel (top) 1525.05 m/s water vel (7 m) 1523.24 m/s water vel (bot) 1521.24 m/s	water depth 15 m density 1.7 g/cm^3
13 SNAP	Y	4.48e-2	3000 3	P-vel (4 shape funcs.) P-att 0.25 dB/λ P-att 0.25 dB/λ source depth 6.06 m roughness (top) 0.03 m roughness (bot) 0.05 m water vel (top) 1525.9 m/s water vel (7 m) 1522.5 m/s water vel (bot) 1524.2 m/s	water depth 15 m density 1.7 g/cm^3
14 OASES[1]	Y	5.40e-2	10000 15	P-vel (4 shape funcs.) P-att (4 shape funcs.)	water depth 15 m water vel 1523 m/s density 1.7 g/cm^3 source depth 7.00 m
15 OASES[2]	Y	6.09e-2	3000 8	P-vel (4 shape funcs.) P-att (3 shape funcs.)	water depth 15 m water vel 1523 m/s density 1.7 g/cm^3 source depth 6.66 m
16 OASES[2]	Y	5.97e-2	2000 5	P-vel (4 shape funcs.) source depth 6.52 m P-att (3 shape funcs.) water depth 15.6 m water vel 1524 m/s	density 1.7 g/cm^3
17 OASES[2]	Y	5.66e-2	2000 5	P-vel (4 shape funcs.) source depth 6.54 m P-att (3 shape funcs.) water depth 14 m water vel 1526 m/s	density 1.7 g/cm^3

[1] Constant layer. [2] Straightline layer.

Report no. changed (Mar 2006): SM-276-UU

Document Data Sheet

NATO UNCLASSIFIED

Security Classification		Project No.
NATO UNCLASSIFIED		19
Document Serial No.	**Date of Issue**	**Total Pages**
SM-276	March 1994	46 pp.

Author(s)

M. Lambert

Title

Inversion of seismo-acoustic real data using genetic algorithms

Abstract

An inversion scheme for the estimation of the physical parameters of marine sediments from the pressure field measured in the water column, is presented. It is based on a global optimization technique called Genetic Algorithms. This report presents results obtained on synthetic and real data. An analysis of the uncertainties of the results is carried out to assess the reliability of the inversion.

Keywords

a posteriori probability distribution, global optimization, genetic algorithm, inverse problems, marine sediment

Issuing Organization

North Atlantic Treaty Organization
SACLANT Undersea Research Centre
Viale San Bartolomeo 400, 19138 La Spezia, Italy

tel: 0187 540 111
fax: 0187 524 600
telex: 271148 SACENT I

[From N. America: SACLANTCEN CMR-426 (New York) APO AE 09613]

Initial Distribution for SM-276

SCNR for SACLANTCEN	
SCNR Belgium	1
SCNR Canada	1
SCNR Denmark	1
SCNR Germany	1
SCNR Greece	1
SCNR Italy	1
SCNR Netherlands	1
SCNR Norway	1
SCNR Portugal	1
SCNR Spain	1
SCNR Turkey	1
SCNR UK	1
SCNR US	2
French Delegate	1
SECGEN Rep. SCNR	1
NAMILCOM Rep. SCNR	1

National Liaison Officers	
NLO Belgium	1
NLO Canada	1
NLO Denmark	1
NLO Germany	1
NLO Italy	1
NLO Netherlands	1
NLO UK	3
NLO US	4

Total external distribution	30
SACLANTCEN Library	20
Total number of copies	50